Article

Single-Cell Bacterial Electrophysiology Reveals Mechanisms of Stress-Induced Damage

Ekaterina Krasnopeeva,[1] Chien-Jung Lo,[2] and Teuta Pilizota[1,*]
[1]Centre for Synthetic and Systems Biology, Institute of Cell Biology, School of Biological Sciences, The University of Edinburgh, Edinburgh, United Kingdom and [2]Department of Physics and Graduate Institute of Biophysics, National Central University, Jhongli, Taiwan, Republic of China

ABSTRACT   An electrochemical gradient of protons, or proton motive force (PMF), is at the basis of bacterial energetics. It powers vital cellular processes and defines the physiological state of the cell. Here, we use an electric circuit analogy of an *Escherichia coli* cell to mathematically describe the relationship between bacterial PMF, electric properties of the cell membrane, and catabolism. We combine the analogy with the use of bacterial flagellar motor as a single-cell "voltmeter" to measure cellular PMF in varied and dynamic external environments (for example, under different stresses). We find that butanol acts as an ionophore and functionally characterize membrane damage caused by the light of shorter wavelengths. Our approach coalesces noninvasive and fast single-cell voltmeter with a well-defined mathematical framework to enable quantitative bacterial electrophysiology.

INTRODUCTION

To stay alive, bacteria, like other cells, maintain adequate supplies of free energy and, under various external stresses, attempt to stay viable by distributing it to processes essential for coping with the challenge while simultaneously maintaining core cellular functions. The two main sources of free energy in living cells are ATP molecule and proton motive force (PMF). The ATP molecule is the energy "currency" of living organisms used for biosynthesis and transport. The PMF is a direct consequence of the activity of the electron transport chain or substrate-level phosphorylation and serves as the energy source driving numerous cellular processes: ATP production, motility, and active membrane transport. The two are interlinked; ordinarily, PMF is used to synthesize ATP, but ATP can drive the production of PMF as well (1).

As early as 1791, Luigi Galvani proposed that life processes generate electricity (2,3). However, it took more than a century for Hugo Fricke to measure the capacitance of the biological membrane (4) and for Peter Mitchell to explain that PMF is an electrochemical gradient of protons across the membrane that powers the production of ATP (5). PMF consists of two components: pH difference between cytoplasm and the external environment ($\Delta pH = pH_{in} -$

pH_{out}) and the electrical potential across the membrane (V_m; we note that the build-up of the charge occurs at nanometer-thin layer close to the biological membrane (6)).

$$PMF = V_m - \frac{2.303kT}{e}\Delta pH, \qquad (1)$$

where k is the Boltzmann constant, T is the temperature, and e is the elementary charge.

Because life generates electricity used to power its processes and the cell membrane acts as a capacitor, it is reasonable to represent the rest of the cell components with an electrical circuit analogy (7,8) (Fig. 1 A). Then, proton fluxes are currents, oxidative or substrate-level phosphorylation can be considered as an imperfect battery with nonzero internal resistance, and the membrane resistance and capacitance are connected in parallel. Membrane voltage in this analogy is equivalent to the drop of potential on the external resistance. Cytoplasmic pH of *Escherichia coli* is kept within the pH 7.2–7.8 range (9–11). Thus, a cell placed in an external environment whose pH matches its internal pH has a negligible contribution of the pH difference to the total PMF, and V_m in the circuit becomes equivalent to the PMF (see Eq. 1).

The circuit analogy in Fig. 1 A gives a mathematical framework that helps us understand cellular free energy maintenance in a range of different conditions. For example, we can predict changes in V_m when circuit parameters
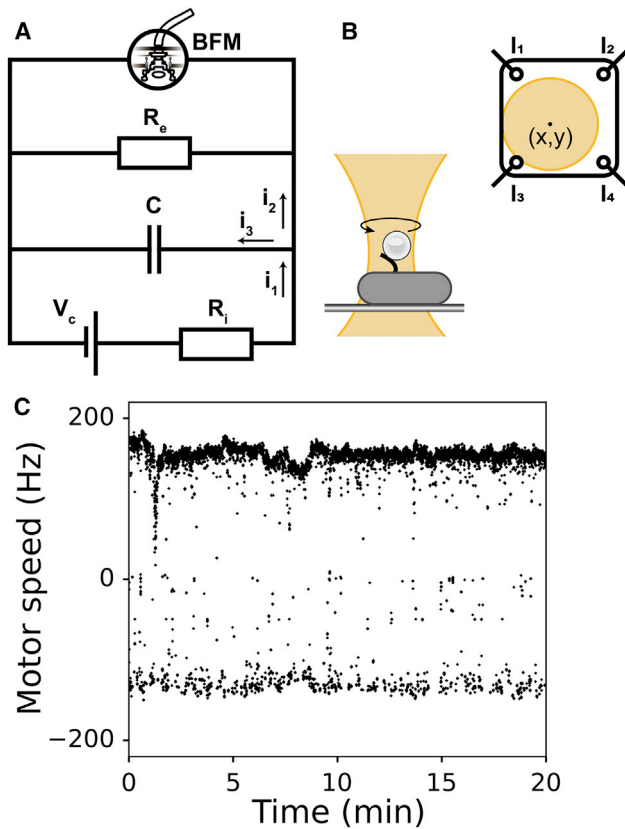
FIGURE 1 (*A*) Electric circuit equivalent of an *E. coli* cell. Oxidative (or substrate-level) phosphorylation is shown as a battery V_c with an internal resistance R_i, the membrane with capacitance C and resistance R_e, and i_1 to i_3 are the currents. Bacterial flagellar motor (BFM) is shown as a "voltmeter" that measures membrane potential, V_m. (*B*) Shown is a schematic of the "bead-assay" and back focal-plane interferometry. A cell is attached to a cover glass with a truncated flagellar filament made "sticky" to polystyrene beads. The bead is brought into a heavily attenuated optical trap, and its position is measured with position sensitive detector. I_1 to I_4 indicate currents read by the position-sensitive detector at four different locations (see Materials and Methods). (*C*) An example of raw motor speed trace recorded with back focal-plane interferometry is shown. Positive frequencies correspond to counterclockwise and negative to the clockwise rotation of the flagellar motor (27). In the subsequent figures, we show absolute values of the rotational speeds. To see this figure in color, go online.

change; a battery depends on the available carbon source, and internal resistance R_i increases in the presence of electron transport chain inhibitors (such as sodium azide (12)). Furthermore, if we could measure V_m with an equivalent of a "voltmeter," we could predict the mechanism and dynamics of the damage as the cells are exposed to various external stresses as well as obtain functional dependence between the affected circuit parameters and the amplitude of the stress.

Here, we report the use of bacterial flagellar motor (BFM) as such a "voltmeter." BFM is a nanomachine that enables bacterial swimming (13) via PMF-powered rotation (14–17). The motor structure and function have been a topic of active research for several decades (13); however, BFM

has not yet been applied as an indicator. Because the motor speed varies linearly with PMF (17,18), we reasoned that it can be used as a robust "PMF-meter" that offers high temporal resolution. When combined with an "electrical circuit interpretation" of the cell, such high-precision, noninvasive PMF (V_m) measurements become a powerful new approach needed for quantitative bacterial electrophysiology. We demonstrate it by revealing the mechanisms of damage caused by chosen stresses; we confirm the behavior of a known ionophore (indole) (19), discover that butanol is an ionophore, and quantitatively describe the nature of damage caused by the light of shorter wavelengths.

MATERIALS AND METHODS

E. coli strains

E. coli EK07 strain is constructed as described in Supporting Materials and Methods, which includes a figure with plasmid maps and a table with the primers. Highly motile *E. coli* strain MG1655 with an insertion sequence element in the *flhD* operon (20) is modified to have *fliC* gene replaced by *fliC*[sticky] (21), which produces flagellar filaments that stick to glass or polystyrene surfaces. Additionally, pHluorin (22,23) gene under strong constitutive *Vibrio harveyi* cytochrome C oxidase promoter (24) is placed onto *att*Tn7 site of the chromosome. All the chromosomal alterations are generated using a plasmid-mediated gene replacement technique (25).

E. coli growth and media

EK07 cells are grown in Lysogeny broth (LB) (10 g tryptone, 5 g yeast extract, 10 g NaCl per 1 L). The overnight culture (optical density (OD) = 5.5) frozen and stored at $-80°C$ in the presence of 20% glycerol is thawed and diluted in a fresh LB to the OD $\approx$ 0.003 (1×1000 dilution from the overnight culture) and grown at $37°C$ with shaking (220 rpm $\times$ g) to OD = 2.0 (Spectronic 200E Spectrophotometer; Thermo Fisher Scientific, London, UK). The OD at harvest is chosen to maximize the number of motors per cell (26) and, thus, increase the yield of the single motor experiments. Growth curves of the EK07 and the parent MG1655 strain are given in Fig. S1. After, growth cells are washed (three times by centrifugation at $8000 \times g$ for 2 min) into MM9 (aqueous solution of 50 mM Na_2HPO_4, 25 mM NaH_2PO_4, 8.5 mM NaCl, and 18.7 mM NH_4Cl with added 0.1 mM $CaCl_2$, 1 mM KCl, 2 mM $MgSO_4$, and 0.3% D-glucose) adjusted to pH 7.5 or PBS (aqueous solution of 154 mM NaCl, 5 mM Na_2HPO_4, and 1.5 mM KH_2PO_4) adjusted to pH 7.5. Indole treatment is performed in MM9 and butanol and photodamage experiments in MM9 and PBS.

Microscope slides preparation

To shorten flagella, cells are "sheared" as described previously (27,28) and washed as above. For butanol and indole treatment, tunnel slides are prepared as before ((28), see also Fig. S2 A). For photodamage experiments, flow cells are manufactured by drilling (Acerdent, London, UK) two 1.8 mm holes on opposite ends of the microscope slide and attaching Tygon R Microbore tubing (Saint Gobain Performance Plastics, Courbevoie, France). The flow cell is then created by attaching a gene frame (Thermo Fisher Scientific) to the slide and covering it with a cover glass (Fig. S2 B). The surface of the cover slide is coated with 0.1% poly-L-lysine by flushing poly-L-lysine through the flow-cell/tunnel-slide for ~10 s, followed by washing it out with the excessive volume of growth medium. The surface coating protocol we are using does not result in an observable growth rate nor internal pH changes when compared to growth on an

agarose pad in the same medium (29). Sheared and washed cells are then loaded into the flow cell/tunnel slide and incubated for 10 min to allow attachment. Excessive cells are washed out with the growth medium. Subsequently, 0.5 mm in diameter polystyrene beads (Polysciences, Warrington, PA) in either PBS or MM9 are added to the flow cell/tunnel slide and incubated for 10 min with consequent washing out of the nonattached beads.

Microscopy and data collection

Back focal-plane interferometry (30,31) is performed as previously described (28). Briefly, heavily attenuated optical trap (855 nm laser) is used to detect the rotation of a polystyrene bead attached to a truncated flagellar filament (Fig. 1 B). Time course of the bead rotation is recorded with the position-sensitive detector (Model 2931; New Focus, Irvine, CA) at 10 kHz, and a 2.5 kHz cutoff antialiasing filter is applied before processing (Fig. 1 B). Bead position (x, y) is calculated from photocurrents $I_1 - I_4$ as $(I_1 + I_2 - (I_3 + I_4))/(I_1 + I_3 + I_2 + I_4) = 2x/L$ and $(I_1 + I_3 - (I_2 + I_4))/(I_1 + I_3 + I_2 + I_4) = 2y/L$, where L is the position-sensitive detector side length.

Fluorescent images of pH-sensitive pHluorin are taken in the same custom-built microscope with iXon Ultra electron-multiplying charge-coupled device camera (Andor, Belfast, UK). OptoLED Dual (Cairn Research, Faversham, UK) independently driving two light-emitting diodes (LEDs) is used for the illumination. Narrow spectrum ultraviolet LED is used for excitation at 395 nm and Neutral White LED with ET470/40x filter (Chroma Technology, Bellows Falls, VT) for 475 nm excitation. Emission is taken at 520 nm using ET525/40× filter (Chroma Technology). Exposure time is fixed at 50 ms for butanol and indole treatment experiments and varies from 10 to 200 ms for photodamage experiments.

Applying stresses

1-Butanol for molecular biology, ≥99%, and indole, analytical standard, are obtained from Sigma-Aldrich (St. Louis, MO). Indole is prepared from a 1 M stock solution in 98% ethanol. The highest concentration of ethanol in the indole solution used for treatment is 0.25%, which by itself does not affect motor speed significantly (see Fig. S3). Treatment is performed as follows: after recording the motor speed for 2 min, 20 mL of MM9 (or PBS) supplemented with a given concentration of butanol or indole is flushed into the tunnel slide. Flush is done by placing a droplet of liquid on one and collecting it with a piece of tissue paper on the other side of the tunnel (32). Duration of the flush is no longer than 10 s. 10 mL droplets of shocking solution are then placed on both sides of the tunnel to minimize evaporation. The shock motor speed is recorded for 10 min, followed by a flush back into MM9 (or PBS) medium. Postshock speed is recorded for 5 min. The motor speed recording is uninterrupted for the duration of the experiment (total of 17 min). For pH control experiments, fluorescent images are taken every 90 s. Control flushes with media containing no indole/butanol are shown in Fig. S4.

Photodamage experiments are performed as follows: using the flow cell, MM9 or PBS is constantly supplied at 10 mL/min rate with a syringe pump (Fusion 400; Chemyx, Stafford, TX). Cells are sequentially exposed to the light of $\lambda = 395$ and 475 nm. Speed recording starts simultaneously with the light exposure. The camera exposure time (tcam) and sampling rate are controlled with a custom written LabView program. tcam are set the same for both wavelengths; however, hardware adds a different delay. Thus, effective light exposure times are tlight $= 225$ ms $+$ tcam for 475 nm and 55 ms $+$ tcam for 395 nm. We record tlight and the sampling rate throughout the experiment to calculate the effective light power (P_{eff}) as the total energy delivered, divided by the total length of the individual motor speed recording. Total energy delivered is estimated by measuring the illumination power in the sample plane multiplied by the total time of light exposure and divided by the illumination area. We measured the illu-

mination area by photobleaching part of the slide and measuring the diameter of the bleached region (d ≈ 220 mm). Control speed traces with no light exposure are shown in Fig. S5.

Data analysis

A flat-top window discrete Fourier transform (window size $= 16,384$ data points with a step dt $= 0.01$ s) is applied to x and y coordinates of a bead position to obtain a time series motor speed record. We refer to this speed record as raw speed traces (Figs. 1 C, 2 A, 3 A, and 4 A; Figs. S3–S5, S8, and S9). Raw traces are further processed as follows: 1) absolute values are taken; 2) values below 10 Hz are removed, and 50 Hz alternating current frequency values disregarded; and 3) remaining data points are median filtered with 201 points moving window. To calculate mean speeds, we apply a 10 s moving window on the speed traces processed as above. In addition to above, photodamage traces are normalized. First, 30 s of the trace is split into 60 windows containing 50 points each. The mean of maximal values found within each window is calculated and considered the initial speed value, by which the rest of the trace is normalized. Each normalized trace is fitted with a single parameter exponential: $y = e^{-\alpha t}$. For Figs. 2 D and 3 D, hyperbolic function fitted is $y = 1/Kx + 1$ and quadratic hyperbolic is $y = 1/Kx^2 + 1$, where K is a fitting parameter. All fittings are performed in Python (SciPy module, curve fit optimization) with a maximal number of calls to the optimization function taken as 20,000. In the Supporting Materials and Methods, we give details on pHluorin image analysis and calibration (including the in vivo and in vitro calibration curves).

RESULTS

PMF measurements via flagellar motor speed can be used to analyze stress-induced damage

The electric circuit analogy (Fig. 1 A) gives a mathematical framework needed to understand cellular free energy maintenance in a range of different conditions. For example, under given external stress, it allows us to 1) discern the affected component of the cell represented in the circuit in Fig. 1 A and 2) predict the mechanism of damage caused by the stress. To pin down the affected component of the cell, we reason in the following manner. Membrane capacitance is set by the geometry of the lipid bilayer and unlikely to be altered on shorter timescales. V_c is the theoretical maximal potential a cell can generate in a given environment and from a given internalized (carbon) source. Stress can affect V_c only by damaging specific carbon transporters, and, thus, it is media dependent. Furthermore, in starvation buffer in which *E. coli* uses internal carbon sources (33), V_c will not be changed by the stress. R_i defines the inefficiency of the catabolism, comprising the drop from V_c as a specific carbon source gets metabolized via a large number of catabolic enzymes. Because these enzymes are at least partially carbon-source specific, the stress that targets R_i will be media dependent. Finally, although the R_e value is growth media dependent, the membrane targeting stresses that influence R_e will be media independent.

Once we pin down the affected component, we employ Kirchoff's laws to express it as a function of stress-induced membrane potential change ($V_m/V_{m,0}$), which we measure
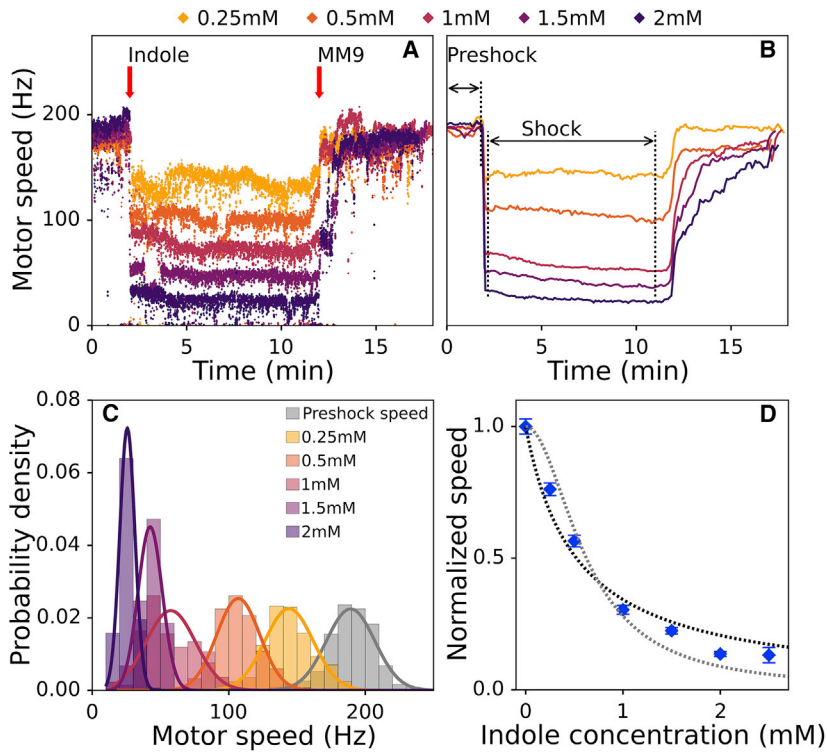
FIGURE 2 BFM speed drops rapidly and increasingly with an increasing indole concentration. (*A*) Examples of raw motor speed traces at five different indole concentrations are shown. Indole is delivered into the tunnel slide 2 min after the recording commences and removed after 12 min. (*B*) Mean speeds of n ≥ 20 motor speeds for each indole concentration are shown against time. Each motor recording is performed on a different cell; thus, the number of motors corresponds to the number of different individual cells. Preshock speed is calculated for the time interval between 0 and 110 s (indicated in the figure). Shock speed is calculated from the 130 to 660 s of the motor recording. Preshock and shock intervals were chosen to exclude the duration of the flush. SEs are given but not visible (for SDs, see Fig. S7 A). (*C*) Probability density of motor speeds for each indole concentration is shown. Experimental data are fitted with a Gaussian probability density function. (*D*) Normalized BMF speeds are plotted against indole concentration. Error bars represent the SE of the mean, and dotted lines show the hyperbolic (*black*) and quadratic hyperbolic (*gray*) fit ($R^2 = 0.97$ and $R^2 = 0.95$, respectively). To see this figure in color, go online.

using BFM as a "voltmeter" (Fig. 1 A). Whereas BFM can be actively slowed down (e.g., when cells enter the stationary phase (34)) on shorter timescales, the linearity between the motor speed (ω) and PMF allows us to use ω as a PMF indicator and, when $pH_{in} \approx pH_{out}$, as a V_m indicator as well. Here, we consider only the situation where $\Delta pH \approx 0$, which we set by adjusting the external pH to the known internal pH of *E. coli* (9), and, in the rest of the text, use PMF and V_m interchangeably. In addition, EK07 strain we constructed (see Materials and Methods) carries a chromosomal copy of the gene-encoding pHluorin protein, which we use to check that our expectation is correct. Fig. S6 shows that throughout the measurements, $\Delta pH \approx 0$ and that the maximal difference in pH units we occasionally observe is maximal at 0.5. This pH gradient at room temperature is equivalent to ~30 mV of PMF, which we consider negligible as it lies within our measured SD. We thus have the following:

$$\omega = \xi * PMF = \xi * V_m, \qquad (2a)$$

$$\frac{\omega}{\omega_0} = \frac{PMF}{PMF_0} = \frac{V_m}{V_{m0}} = f(S, t), \qquad (2b)$$

where we assumed that ω changes as a function of stress amplitude and time f(S, t), ξ is a constant, and index 0 denotes the variable value before stress. We measure ω using back focal-plane interferometry (31) and a polystyrene bead attached to a short filament stub (see Materials and Methods; Fig. 1 B) (27). An example trace of BFM speed

is given in Fig. 1 C. Using Eq. 2b and the circuit analogy, we can express each circuit component as a function of stress. To do so, we simplify the electric circuit by estimating the RC constant of the cell membrane. Capacitance and resistance of the bacterial membrane have been reported as C ≈ 1 mF/cm^2 (35,36) and R ≈ 10–1000 Ω*cm^2 (19,37), which gives RC in the range of 10^{-5}–10^{-3} s. Thus, the current through the capacitor (i_3) is zero before the stress application (when the system is in steady state) as well as poststress application when $t > 1$ ms (less than our experimental resolution). Next, we consider ΔG of nicotinamide adenine dinucleotide oxidation only and compute that the respiratory chain can produce $V_c \approx -360$ mV (8). Yet, the physiological value of the membrane potential of respiring bacteria is approximately equal to −160 mV (38), indicating that roughly half of the membrane potential drops at the internal resistance (i.e., $R_{i,0} \approx R_{e,0}$). Taking the two simplifications into account, we arrive to the following (see Fig. 1 A; Supporting Materials and Methods for a detailed deduction of equations):

$$\frac{V_c}{V_{c0}} = f(s, t), \qquad (3a)$$

$$\frac{R_i}{R_{i0}} = \frac{2}{f(S, t)} - 1, \qquad (3b)$$

$$\frac{R_e}{R_{e0}} = \frac{f(S, t)}{2 - f(S, t)}. \qquad (3c)$$
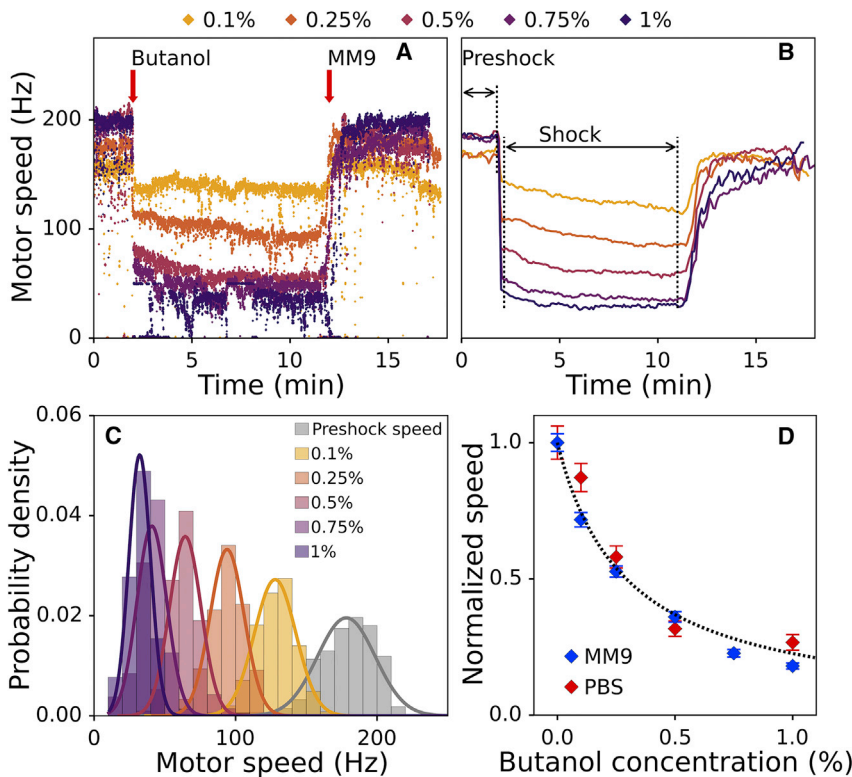
FIGURE 3 BFM speed drops sharply and reversibly after butanol treatment. (A) Examples of raw BFM speed traces for five different butanol concentrations are shown. Butanol is delivered 2 min into the recording and removed after 12 min. (B) Mean speeds of n $\geq$ 20 cells per different butanol concentrations are plotted against time. Preshock and shock speeds are calculated in the 0–110 s and 130–660 s time interval, respectively. SEs of the mean are given but not visible. SDs of the same traces are given in Fig. S7 B. (C) Probability densities of shock speed for each butanol concentration and the preshock speed are shown. (D) Shock speeds obtained from the distributions are normalized by the preshock speed and plotted against butanol concentration. Blue diamonds show the cells in MM9 media, and red diamonds show the cells in PBS. Error bars represent SE of the mean. Hyperbolic fit is given as a black dotted line ($R^2 = 0.96$). To see this figure in color, go online.

Eqs. 3a, 3b, and 3c allow us to relate changes in BFM speed and thus cellular PMF, with the changes in the components of the electric circuit presented in Fig. 1 A. To start, we included only high-level features of the cell. However, a more detailed representation of the cell in the circuit analogy is possible (e.g., external resistance may be split into parallel resistances representing lipids or specific membrane proteins).

PMF dynamics analysis confirms indole is an ionophore

We test the proposed circuit analogy and applicability of the BFM speed as the voltmeter by applying a known membrane stress. We choose a cell signaling molecule indole that, at millimolar concentrations, forms a dimer and acts as an ionophore (19). Ionophores are molecules that carry ions across the lipid bilayer; thus, we expect the membrane
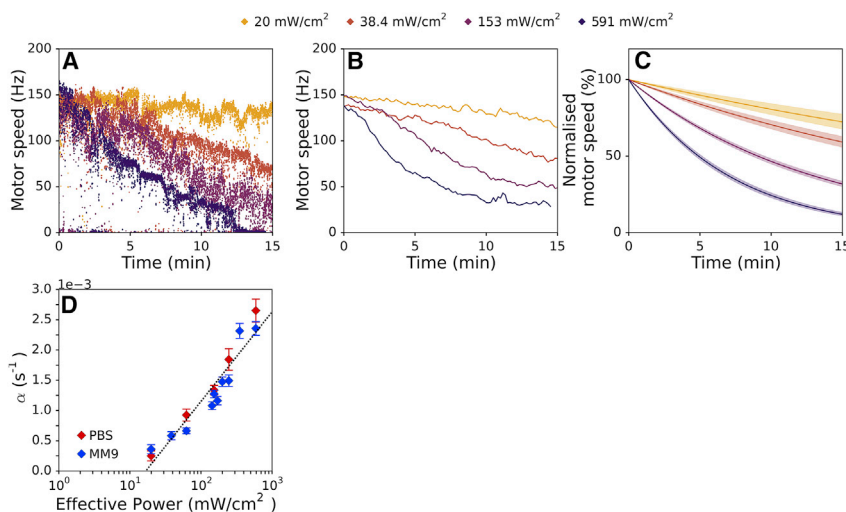
FIGURE 4 Rate of the motor speed decay increases with the light power. (A) Examples of raw traces at four different effective powers are shown (P_{eff} = 20, 38.4, 153, or 591 mW/cm^2). (B) Shown is the mean BFM speed at different illumination powers (21–34 cells are recorded per condition). (C) Averaged exponential fits for different illumination powers with SE are shown. Each individual motor trace is fitted with an exponential function, and the mean of fitting parameter α is calculated for each P_{eff}. (D) Exponential fit coefficient α is plotted against illumination power. Blue diamonds show the cells in MM9 media, and red diamonds show the cells in PBS. Error bars represent SE, and the dotted line represents the logarithmic fit ($R^2 = 0.906$). The total number of cells in MM9 is 277 and in PBS is 116. To see this figure in color, go online.

resistance to decrease (ion conductance increases) when indole is present in the medium. Furthermore, we expect to recover previously demonstrated parabolic dependence of membrane conductance on indole concentration (19).

Fig. 2 A shows examples of individual motor speed recordings before, during, and post-treatment with a given concentration of indole. Motor speed drops immediately with the addition of indole and stays at approximately the same level until indole is removed, at which point it recovers to the initial level. The speed change caused by indole is faster than 10 ms (our experimental resolution), confirming the estimate of the membrane RC constant and justifying the assumption that the current through the capacitance in the Fig. 1 A circuit is negligible. Indole solution used for the treatment contains a low percentage of ethanol (up to 0.25%). Fig. S3 shows that traces of ethanol do not significantly affect the motor speed if indole is not present.

To confirm the dependence of the membrane resistance on indole, we find the relative change in motor speed at a given stress concentration. Fig. 2 B shows the mean speed traces for different indole concentrations (see Materials and Methods for mean speed calculation), and in Fig. 2 C, we plot the probability densities of preshock and shock speeds. From the Gaussian fits to preshock and shock speed distributions, we obtain mean shock speeds for a given indole concentration and plot them normalized to the preshock speed (Fig. 2 D). We fit the normalized speeds with hyperbolic or quadratic hyperbolic function (see Materials and Methods, both of which yield good quality fits with R^2 higher than 0.90). The concentrations of indole at which the quadratic dependence becomes particularly obvious in previous study range between 2 and 5 mM (19), whereas we observe a significant effect in the 0–2.5 mM range. The difference can be explained by variations in electrochemical properties of cells and kept or grown in different media and to a different growth stage. Another possible reason is a residual accumulation of indole in a cell membrane, which has been reported in wild-type indole-producing cells grown to a late exponential phase (39) (Chimerel et al. in their work used an indole-nonproducing strain (19)). However, BFM speed recovers to the same level after indole removal (Fig. 2). Thus, if there is a residual accumulation of indole, it is kept constant during the experiments.

Butanol acts as an ionophore, changing membrane conductance linearly with concentration

To determine the mechanism of action of an unknown stress, we choose butanol. Previous work indicates that butanol interacts with the cell membrane and weakens it, but the exact mechanism of the cell damage is unknown (40).

We perform the BFM speed measurements in *E. coli* cells treated with butanol. The experimental protocol of butanol delivery is the same as for indole. Fig. 3, A and B show ex-

amples of raw traces and mean speed traces before, during, and after butanol shock in MM9. Immediately upon butanol stress, motor speed drops, and upon butanol removal, it recovers to the initial value (Fig. 3 A). Motor speed distributions at a given butanol concentration remain narrow, and we fit them with Gaussian curves (Fig. 3 C). Fig. 3 D shows normalized motor speeds, calculated as mean values of the distributions given in Fig. 3 C and plotted against butanol concentration for both MM9 media and PBS.

The relative speed drop observed in the presence of butanol is media independent and like that observed for indole. The finding suggests that, on the timescale of our experiment, butanol causees nonpermanent membrane damage and acts as an ionophore. The normalized motor speed dependence on butanol concentration is hyperbolic, and we obtain Eq. 3c for membrane resistance:

$$R_e = \frac{R_{e0}}{7.8c_{but} + 1}, \tag{4}$$

where c_{but} is a butanol concentration in percentage and 7.8 is a value of constant K obtained from the hyperbolic fit (see Materials and Methods). We observe the speed restoration after butanol removal even after multiple treatments of the same cell. Fig. S8 shows several consecutive butanol stresses, each lasting 60 s (Fig. S8 A) or 30 s (Fig. S8 B), in which after each treatment, motor speed is fully restored.

Photodamage increases membrane conductance that scales with the light power

As an example of a complex stress, we next choose to characterize light-induced damage. Although previous reports indicate that light causes wavelength-dependent damage to bacterial cells (41,42), they also suggest that the nature of damage is complex. Most likely, the cause of the damage is the formation of reactive oxygen species (ROS) (43,44), which have been shown to perturb multiple components of the cell: DNA, RNA, proteins, and lipids (45,46). To apply light of a certain wavelength and intensity to bacterial cells, we use a flow cell (see Materials and Methods). During the light exposure, cells are continuously supplied with fresh media at 10 mL/min of flow rate. We apply the light of 395 and 475 nm wavelengths as the choice allows us to simultaneously measure the internal pH of bacteria.

Fig. 4 A shows example BFM speed traces during exposure to light of different effective powers (P_{eff}) delivered to the cells. P_{eff} is calculated as the total energy delivered divided by the total time the light is on (see Materials and Methods). Fig. 4 A shows that BFM speed gradually decreases in time during exposure to light and that the decrease rate scales with the P_{eff}, also visible in Fig. 4 B, showing mean BFM speed traces for the same four effective powers.

To identify the functional dependence of the speed decrease rate on P_{eff}, we fit individual normalized traces

with the simple exponential function: $\omega/\omega_0 = e^{-\alpha t}$, with the single fitting parameter α. Mean of the fits with SEs at corresponding four different powers are shown in Fig. 4 C, and Fig. 4 D shows the fit coefficient α plotted against the light power for both MM9 medium and PBS. The effect of light on V_m is present in PBS and of the same functional dependence; thus, on the timescales of our experiment, light affects primarily the membrane resistance, R_e. Together with the fact that the speed decrease rates stay the same at a given P_{eff}, the finding suggests that on the timescale of our experiment, there is no active membrane repair. We further confirm this by measuring the motor speed after we expose the cells to light for shorter periods of time. Fig. S9 shows that when the illumination ceases after 5 or 15 min, the (decreased) BFM speed remains the same with no visible recovery. We also check that light damage is not enhanced by the presence of the fluorescent protein (pHluorin) in the cytoplasm (Fig. S10).

Fig. 4 D enables us to determine the functional relationship between the effective power and α, which increases as a logarithm of the normalized P_{eff} (i.e., $P_{eff,norm} = P_{eff}/(mW \times cm^{-2})$). Thus, for our initial exponential fit, we obtain the following:

$$\omega = \omega_0 e^{-(a \ln P_{eff,norm} + b)t}, \qquad (5)$$

where a and b are wavelength-specific parameters, $a = 0.00064$ s^{-1} and $b = -0.00181$ s^{-1}, and Eq. 5 holds for $P_{eff} > P_{eff,0}$.

The minimal power required for the damage to occur is defined as $P_{eff,0} = e^{-b/a}$ mW/cm^2, and for 395 and 475 nm, this is $\sim$17 mW/cm^2. Rewriting Eq. 5 in terms of $P_{eff,0}$, we get the following:

$$\omega = \omega_0 \left(\frac{P_{eff0}}{P_{eff}}\right)^{at} \qquad (6)$$

Finally, applying Eq. 6 to Eq. 3c, we derive R_e functional dependence on the effective power:

$$R_e = \frac{R_{e0}}{2\left(\frac{P_{eff}}{P_{eff0}}\right)^{at} - 1}, \qquad (7)$$

where a is the fit coefficient in Fig. 4 D.

DISCUSSION

Arguably, one of the defining features of life is its ability to avoid thermodynamic equilibrium (death) by achieving a steady-state supply of free energy. Chemiosmotic theory explained that the production of life's energy currency, the ATP molecule, proceeds via the generation of transmembrane electrochemical potential. The ability to measure and control the voltage and current across the cellular membrane with the patch-clamp technique had far-reaching con-

sequences for our understanding of cells such as neurons, in which the electrical inputs govern signal transmission (36). In the cases of bacteria and their small size, we are unable to gain the same level of control over these parameters (47,48), despite the fact that the ability to do so would open a range of currently inaccessible questions that are at the basis of bacterial free energy maintenance and, consequently, survival.

Here, we demonstrate the use of BFM as a fast voltmeter, enabling quantitative in vivo studies of electrochemical properties of the bacterial membrane. Alternative methods for measuring V_m in E. coli rely on fluorescent readout (49–51). However, Nernstian dyes (49,50) sometimes fail to penetrate E. coli's membrane (52), can be a substrate for the outer membrane efflux system TolC (53), and in external conditions in which they do equilibrate across the membrane, they do so on the timescales of minutes (52,54). Voltage-sensitive membrane proteins that can be used in E. coli require the delivery of the light of the high power (51). BFM, on the other hand, is native to E. coli and expressed in a range of conditions (J. Cremer, T. Honda, Y. Tang, J. Ng, M. Vergassola, and T. Hwa, personal communication). Speed measurements via back focal-plane interferometry or fast cameras do not rely on fluorescent illumination and offer high time resolution (up to 0.5 ms (55)).

We choose to work with cells grown into the late exponential phase in LB because this has been shown to maximize the number of motors expressed per cell (26). However, our methodology is applicable across a range of growth conditions. Cremer et al. demonstrate that cells in steady-state (exponential) growth express motors in both rich and poor media (J. Cremer, T. Honda, Y. Tang, J. Ng, M. Vergassola, and T. Hwa, personal communication). To obtain steady-state growth, cells from an overnight (stationary) culture need to divide a sufficient number of times before running out of nutrients, which is easiest achieved by ample dilutions into the fresh media. We expect that the cells grown in different media will have different electrochemical properties, which can be measured with our approach in the future.

In this work, we choose conditions that satisfy ΔpH $\approx$ 0, and thus, V_m is the only contribution to the PMF. However, BFM speed measurements can be extended to conditions in which the ΔpH contribution to the PMF is not negligible; V_m in this case will be calculated from Eq. 1. Extending the use of BFM as the voltmeter for long-term measurements (into hours and days) is possible. We note that on longer timescales, the motor can be actively slowed down via YcgR protein (34,56), and such long-term measurements would likely require YcgR deletion background. We also note that we have assumed that only one of the components of the circuit is affected by the stress as most stresses predominantly act on one of the circuit components immediately postapplication. To apply the approach to the stresses that change two or more components at a time,

further assumptions regarding the stress function will be required to introduce additional equations into the circuit model.

We base the use of BFM as the cell's voltmeter on the proportionality between motor speed and PMF, measured first more than 20 years ago (17,18). Recent experiments show that BFM also exhibit mechanosensing (57,58), in which stator unit incorporation depends on the motor torque. These recent findings indicate an intriguing control mechanism, in which mechanosensing and the ion flux combined result in the characteristic proportional relationship between the BFM speed and PMF. It will be interesting to fully ascertain the exact molecular mechanism behind the PMF-motor speed relationship, and we think the ability to fine control the PMF loss can contribute to that understanding.

Using the electric circuit analogy for the membrane fluxes and BFM as the cell's "voltmeter," we demonstrate the effect of three different stresses on the cell's membrane conductance. For the known stress, indole, we confirm it acts as an ionophore. For the first unknown stress we applied, butanol, we show its presence decreases membrane resistance, inversely proportional to the butanol concentration. Thus, we conclude that, in the concentration range we tested and on the 15 min timescale, butanol behaves as an ionophore in a manner similar to indole or carbonyl cyanide m-chlorophenyl hydrazone (19). With an analysis like we presented, butanol action can be characterized further (e. g. defining the minimal concentration and incubation time required for the effect to become irreversible). For our last stress, the light of short wavelengths, we show that it affects membrane resistance and functionally describe the damage in relation to time and P_{eff}. Light-induced changes in membrane permeability have been reported in artificial planar lipid bilayer systems and liposomes in the presence of photosensitizers (59–62).

The most likely cause of such changes is ROS-induced chain-reaction lipid peroxidation (63–67). The presence of peroxidized lipids can change the bilayer physical and electrical properties (68–70) (e.g., it has been suggested that it induces the formation of hydrophobic prepores and their later transformation into hydrophilic pores permeable to ions) (61,62). Based on the previous work and our real-time in vivo measurements, we propose the following model for the complex nature of the light-induced membrane damage. Exposure to light causes the formation of ROS that induce lipid peroxidation and thus alter the electrical properties of the membrane. In particular, its permeability to ions is due to the formation of hydrophilic pores. In contrast to the ionophores that carry ions across the membrane without causing membrane damage, the drop in V_m we observe under light proceeds as a result of a slower, multistep formation of lipid pores that require active repair to be mitigated. Therefore, we do not see any fast recovery after illumination ceases (Fig. S9).

Living cells have built-in mechanisms of coping with oxidative stress (for example, SoxRS/OxyR regulons containing multiple antioxidant-encoding genes, such as *sodA* (manganese superoxide dismutase) or *katG* (hydroperoxidase I)) (70,71). The existence of defense mechanisms explains the occurrence of the minimal power required to cause the damage. Less power, even if it causes ROS formation, will not damage the cells that cope using internal protection enzymes. The value of the minimal damage-causing power we measured can indicate the abundance of internal protective resources available to the cell as well as define the power range for fluorescence imaging that should be used to ensure that no (unaccounted for) damage is inflicted to the cells by the exposure to light.

Future applications of our approach include, but are not limited to, studying other damage mechanisms and characterizing unknown bacterial membrane properties (e.g., overall resistance in different growth conditions). Last, based on our measurements, we suggest the use of light for the delivery of small molecules, such as antimicrobial peptides or fluorescent dyes, which otherwise fail to penetrate *E. coli*'s membrane (52).

Raw data generated as part of this work are available at https://datashare.is.ed.ac.uk/handle/10283/2058.

SUPPORTING MATERIAL

Supporting Material can be found online at https://doi.org/10.1016/j.bpj.2019.04.039.

AUTHOR CONTRIBUTIONS

E.K., C.-J.L., and T.P. designed research. E.K. performed research and analyzed data. E.K., C.-J.L., and T.P. interpreted results and wrote the article.

ACKNOWLEDGMENTS

SUPPORTING CITATIONS

References (72–77) appear in the Supporting Material.

REFERENCES

1. Keis, S., A. Stocker, …, G. M. Cook. 2006. Inhibition of ATP hydrolysis by thermoalkaliphilic F1Fo-ATP synthase is controlled by the C terminus of the epsilon subunit. *J. Bacteriol.* 188:3796–3804.

2. Galvani, L. 1791. De viribus electricitatis in motu musculari commentarius, De Bononiensi Scientiarum et Artium Instituto atque: Academia Commentarii, tomus septimus, pp. 363–418.

3. Green, R. M. 1953. A translation of Luigi galvani's de viribus electricitatis in motu musculari commentarius. Commentary on the effect of electricity on muscular motion. *J. Am. Med. Assoc.* 153:989.

4. Fricke, H. 1923. The electric capacity of cell suspension. *Phys. Rev.* 21:708–709.

5. Mitchell, P. 1961. Coupling of phosphorylation to electron and hydrogen transfer by a chemi-osmotic type of mechanism. *Nature.* 191:144–148.

6. Nelson, P. C. 2003. Biological Physics: Energy, Information, Life. W. H. Freeman, New York.

7. Van Rotterdam, B. J., W. Crielaard, …, H. V. Westerhoff. 2002. Simplicity in complexity: the photosynthetic reaction center performs as a simple 0.2 V battery. *FEBS Lett.* 510:105–107.

8. Walter, J. M., D. Greenfield, …, J. Liphardt. 2007. Light-powering Escherichia coli with proteorhodopsin. *Proc. Natl. Acad. Sci. USA.* 104:2408–2412.

9. Slonczewski, J. L., B. P. Rosen, …, R. M. Macnab. 1981. pH homeostasis in Escherichia coli: measurement by 31P nuclear magnetic resonance of methylphosphonate and phosphate. *Proc. Natl. Acad. Sci. USA.* 78:6271–6275.

10. Zilberstein, D., V. Agmon, …, E. Padan. 1984. Escherichia coli intracellular pH, membrane potential, and cell growth. *J. Bacteriol.* 158:246–252.

11. Wilks, J. C., and J. L. Slonczewski. 2007. pH of the cytoplasm and periplasm of Escherichia coli: rapid measurement by green fluorescent protein fluorimetry. *J. Bacteriol.* 189:5601–5607.

12. Noumi, T., M. Maeda, and M. Futai. 1987. Mode of inhibition of sodium azide on H+-ATPase of Escherichia coli. *FEBS Lett.* 213:381–384.

13. Sowa, Y., and R. M. Berry. 2008. Bacterial flagellar motor. *Q. Rev. Biophys.* 41:103–132.

14. Manson, M. D., P. M. Tedesco, and H. C. Berg. 1980. Energetics of flagellar rotation in bacteria. *J. Mol. Biol.* 138:541–561.

15. Matsuura, S., J. I. Shioi, and Y. Imae. 1977. Motility in Bacillus subtilis driven by an artificial protonmotive force. *FEBS Lett.* 82:187–190.

16. Meister, M., G. Lowe, and H. C. Berg. 1987. The proton flux through the bacterial flagellar motor. *Cell.* 49:643–650.

17. Fung, D. C., and H. C. Berg. 1995. Powering the flagellar motor of Escherichia coli with an external voltage source. *Nature.* 375:809–812.

18. Gabel, C. V., and H. C. Berg. 2003. The speed of the flagellar rotary motor of Escherichia coli varies linearly with protonmotive force. *Proc. Natl. Acad. Sci. USA.* 100:8748–8751.

19. Chimerel, C., C. M. Field, …, D. K. Summers. 2012. Indole prevents Escherichia coli cell division by modulating membrane potential. *Biochim. Biophys. Acta.* 1818:1590–1594.

20. Barker, C. S., B. M. Prüss, and P. Matsumura. 2004. Increased motility of Escherichia coli by insertion sequence element integration into the regulatory region of the flhD operon. *J. Bacteriol.* 186:7529–7537.

21. Kuwajima, G. 1988. Construction of a minimum-size functional flagellin of Escherichia coli. *J. Bacteriol.* 170:3305–3309.

22. Miesenböck, G., D. A. De Angelis, and J. E. Rothman. 1998. Visualizing secretion and synaptic transmission with pH-sensitive green fluorescent proteins. *Nature.* 394:192–195.

23. Morimoto, Y. V., S. Kojima, …, T. Minamino. 2011. M153R mutation in a pH-sensitive green fluorescent protein stabilizes its fusion proteins. *PLoS One.* 6:e19598.

24. Pilizota, T., and J. W. Shaevitz. 2012. Fast, multiphase volume adaptation to hyperosmotic shock by Escherichia coli. *PLoS One.* 7:e35205.

25. Link, A. J., D. Phillips, and G. M. Church. 1997. Methods for generating precise deletions and insertions in the genome of wild-type Escherichia coli: application to open reading frame characterization. *J. Bacteriol.* 179:6228–6237.

26. Amsler, C. D., M. Cho, and P. Matsumura. 1993. Multiple factors underlying the maximum motility of Escherichia coli as cultures enter post-exponential growth. *J. Bacteriol.* 175:6238–6244.

27. Bai, F., R. W. Branch, …, R. M. Berry. 2010. Conformational spread as a mechanism for cooperativity in the bacterial flagellar switch. *Science.* 327:685–689.

28. Rosko, J., V. A. Martinez, …, T. Pilizota. 2017. Osmotaxis in Escherichia coli through changes in motor speed. *Proc. Natl. Acad. Sci. USA.* 114:E7969–E7976.

29. Wang, Y. K., E. Krasnopeeva, …, C.-J. Lo. 2019. Comparison of Escherichia coli surface attachment methods for single-cell, in vivo microscopy. *bioRxiv* https://doi.org/10.1101/648840.

30. Denk, W., and W. W. Webb. 1990. Optical measurement of picometer displacements of transparent microscopic objects. *Appl. Opt.* 29:2382–2391.

31. Svoboda, K., C. F. Schmidt, …, S. M. Block. 1993. Direct observation of kinesin stepping by optical trapping interferometry. *Nature.* 365:721–727.

32. Buda, R., Y. Liu, …, T. Pilizota. 2016. Dynamics of Escherichia coli 's passive response to a sudden decrease in external osmolarity. *Proc. Natl. Acad. Sci. USA.* 113:E5838–E5846.

33. Nyström, T., and N. Gustavsson. 1998. Maintenance energy requirement: What is required for stasis survival of Escherichia coli? *Biochim. Biophys. Acta.* 1365:225–231.

34. Boehm, A., M. Kaiser, …, U. Jenal. 2010. Second messenger-mediated adjustment of bacterial swimming velocity. *Cell.* 141:107–116.

35. Fricke, H., H. P. Schwan, …, V. Bryson. 1956. A dielectric study of the low-conductance surface membrane in E. coli. *Nature.* 177:134–135.

36. Hodgkin, A. L., A. F. Huxley, and B. Katz. 1952. Measurement of current-voltage relations in the membrane of the giant axon of Loligo. *J. Physiol.* 116:424–448.

37. Miyamoto, V., and T. Thompson. 1967. Some electrical properties of lipid bilayer membranes. *J. Colloid Interface Sci.* 25:16–25.

38. Tran, Q. H., and G. Unden. 1998. Changes in the proton potential and the cellular energetics of Escherichia coli during growth by aerobic and anaerobic respiration or by fermentation. *Eur. J. Biochem.* 251:538–543.

39. Gaimster, H., J. Cama, …, D. K. Summers. 2014. The indole pulse: a new perspective on indole signalling in Escherichia coli. *PLoS One.* 9:e93168.

40. Fletcher, E., T. Pilizota, …, C. E. French. 2016. Characterization of the effects of n-butanol on the cell envelope of E. coli. *Appl. Microbiol. Biotechnol.* 100:9653–9659.

41. Ashkin, A., J. M. Dziedzic, and T. Yamane. 1987. Optical trapping and manipulation of single cells using infrared laser beams. *Nature.* 330:769–771.

42. Neuman, K. C., E. H. Chadd, …, S. M. Block. 1999. Characterization of photodamage to Escherichia coli in optical traps. *Biophys. J.* 77:2856–2863.

43. de Jager, T. L., A. E. Cockrell, and S. S. Du Plessis. 2017. Ultraviolet light induced generation of reactive oxygen species. *In* Ultraviolet Light in Human Health, Diseases and Environment. Advances in Experimental Medicine and Biology. S. Ahmad, ed. Springer, pp. 15–23.

44. Lockwood, D. B., J. C. Wataha, …, S. D. Hsu. 2005. Blue light generates reactive oxygen species (ROS) differentially in tumor vs. normal epithelial cells. *Dent. Mater.* 21:683–688.

45. Cabiscol, E., J. Tamarit, and J. Ros. 2000. Oxidative stress in bacteria and protein damage by reactive oxygen species. *Int. Microbiol.* 3:3–8.

46. Zhao, X., and K. Drlica. 2014. Reactive oxygen species and the bacterial response to lethal stress. *Curr. Opin. Microbiol.* 21:1–6.

47. Ruthe, H. J., and J. Adler. 1985. Fusion of bacterial spheroplasts by electric fields. *Biochim. Biophys. Acta.* 819:105–113.

48. Martinac, B., M. Buechner, …, C. Kung. 1987. Pressure-sensitive ion channel in Escherichia coli. *Proc. Natl. Acad. Sci. USA.* 84:2297–2301.

49. Ehrenberg, B., V. Montana, …, L. M. Loew. 1988. Membrane potential can be determined in individual cells from the nernstian distribution of cationic dyes. *Biophys. J.* 53:785–794.

50. Prindle, A., J. Liu, …, G. M. Süel. 2015. Ion channels enable electrical communication in bacterial communities. *Nature.* 527:59–63.

51. Kralj, J. M., D. R. Hochbaum, …, A. E. Cohen. 2011. Electrical spiking in Escherichia coli probed with a fluorescent voltage-indicating protein. *Science.* 333:345–348.

52. Lo, C. J., M. C. Leake, …, R. M. Berry. 2007. Nonequivalence of membrane voltage and ion-gradient as driving forces for the bacterial flagellar motor at low load. *Biophys. J.* 93:294–302.

53. Mancini, L., G. Terradot, …, T. Pilizota. 2019. Escherichia coli's physiology can turn membrane voltage dyes into actuators. *bioRxiv* https://doi.org/10.1101/607838.

54. Te Winkel, J. D., D. A. Gray, …, H. Strahl. 2016. Analysis of antimicrobial-triggered membrane depolarization using voltage sensitive dyes. *Front. Cell Dev. Biol.* 4:29.

55. Pilizota, T., T. Bilyard, …, R. M. Berry. 2007. A programmable optical angle clamp for rotary molecular motors. *Biophys. J.* 93:264–275.

56. Paul, K., V. Nieto, …, R. M. Harshey. 2010. The c-di-GMP binding protein YcgR controls flagellar motor direction and speed to affect chemotaxis by a "backstop brake" mechanism. *Mol. Cell.* 38:128–139.

57. Lele, P. P., B. G. Hosu, and H. C. Berg. 2013. Dynamics of mechanosensing in the bacterial flagellar motor. *Proc. Natl. Acad. Sci. USA.* 110:11839–11844.

58. Tipping, M. J., N. J. Delalez, …, J. P. Armitage. 2013. Load-dependent assembly of the bacterial flagellar motor. *MBio.* 4:e00551-13.

59. McRae, D. G., E. Yamamoto, and G. H. Towers. 1985. The mode of action of polyacetylene and thiophene photosensitizers on liposome permeability to glucose. *Biochim. Biophys. Acta.* 821:488–496.

60. Pashkovskaya, A., E. Kotova, …, Y. Antonenko. 2010. Light-triggered liposomal release: membrane permeabilization by photodynamic action. *Langmuir.* 26:5726–5733.

61. Kotova, E. A., A. V. Kuzevanov, …, Y. N. Antonenko. 2011. Selective permeabilization of lipid membranes by photodynamic action via formation of hydrophobic defects or pre-pores. *Biochim. Biophys. Acta.* 1808:2252–2257.

62. Wong-Ekkabut, J., Z. Xu, …, L. Monticelli. 2007. Effect of lipid peroxidation on the properties of lipid bilayers: a molecular dynamics study. *Biophys. J.* 93:4225–4236.

63. Girotti, A. W. 1985. Mechanisms of lipid peroxidation. *J. Free Radic. Biol. Med.* 1:87–95.

64. Girotti, A. W. 1990. Photodynamic lipid peroxidation in biological systems. *Photochem. Photobiol.* 51:497–509.

65. Halliwell, B., and S. Chirico. 1993. Lipid peroxidation: its mechanism, measurement, and significance. *Am. J. Clin. Nutr.* 57 (5 Suppl):715S–724S, discussion 724S–725S.

66. Heck, D. E., A. M. Vetrano, …, J. D. Laskin. 2003. UVB light stimulates production of reactive oxygen species: unexpected role for catalase. *J. Biol. Chem.* 278:22432–22436.

67. Lavi, R., A. Shainberg, …, R. Lubart. 2010. Detailed analysis of reactive oxygen species induced by visible light in various cell types. *Lasers Surg. Med.* 42:473–480.

68. Dobretsov, G. E., T. A. Borschevskaya, …, Y. A. Vladimirov. 1977. The increase of phospholipid bilayer rigidity after lipid peroxidation. *FEBS Lett.* 84:125–128.

69. Richter, C. 1987. Biophysical consequences of lipid peroxidation in membranes. *Chem. Phys. Lipids.* 44:175–189.

70. Birben, E., U. Murat, …, O. Kalayci. 2012. Oxidative stress and antioxidant defense. *World Allergy Organ. J.* 5:9–19.

71. Storz, G., and J. A. Imlay. 1999. Oxidative stress. *Curr. Opin. Microbiol.* 2:188–194.

72. Merlin, C., S. McAteer, and M. Masters. 2002. Tools for characterization of Escherichia coli genes of unknown function. *J. Bacteriol.* 184:4573–4581.

73. Martinez, K. A., II, R. D. Kitko, …, J. L. Slonczewski. 2012. Cytoplasmic pH response to acid stress in individual cells of Escherichia coli and Bacillus subtilis observed by fluorescence ratio imaging microscopy. *Appl. Environ. Microbiol.* 78:3706–3714.

74. Urh, M., D. Simpson, and K. Zhao. 2009. Affinity chromatography: general methods. *Methods Enzymol.* 463:417–438.

75. Otsu, N. 1979. A threshold selection method from gray-level histograms. *IEEE Trans. Syst. Man Cybern.* 9:62–66.

76. Berg, H. C., and L. Turner. 1993. Torque generated by the flagellar motor of Escherichia coli. *Biophys. J.* 65:2201–2216.

77. Rosko, J. 2017. Osmotaxis in Escherichia coli. The Edinburgh University, PhD thesis.